Article **ECORFAN-Bolivia Journal**
December 2016 Vol.3 No. 5 19-28

Structural characterization of CdS doped with Pb^{2+}

DÍAZ-REYES, J*† ′ , SÁNCHEZ-RAMÍREZ, J.F′, FLORES-MENA, J.E″and MORÍN-CASTILLO, M.M ″

′Center for Research in Applied Biotechnology, Instituto Politécnico Nacional. Ex-Hacienda de San Juan Molino, Km. 1.5. Tepetitla, Tlaxcala. 90700. México
″Faculty of Sciences of the Electronics, Benemérita Universidad Autónoma de Puebla. Av. San Claudio y 18 Sur. Ciudad Universitaria. Puebla, Puebla. 72570. México

Received August 14, 2016; Accepted November 1 2016

Abstract

CdS nanocrystals doped with Pb^{2+} are synthesised using a chemical bath deposition (CBD) growth technique under optimum conditions lead acetate at the reservoir temperature of 20±2°C. The Pb^{2+} molar concentration was of $0.0 \leq x \leq 0.19.67$ that was determined by EDS. The X-ray diffraction results show that the films are of PbS-CdS composites with individual CdS and PbS planes. The XRD analysis and Raman scattering reveal that CdS-deposited films showed zinc blende (ZB) crystalline phase. The mean grain size of the CdS films was ranged from 1.21-6.67 nm that was determined by Debye-Scherrer equation from ZB (111) direction and confirmed by high-resolution transmission electron microscopy (HRTEM). Raman scattering shows that the lattice dynamics is characteristic of bimodal behaviour and the multipeaks adjust of the first optical longitudinal mode for the Pb^{2+}-doped CdS denotes the Raman shift of the characteristic peak in the range of 305-298 cm^{-1} of the CdS crystals, which is associated with the lead ions incorporation.

CBD, Semiconductor compounds II-VI, Raman spectroscopy, XRD

Citation: DÍAZ-REYES, J, SÁNCHEZ-RAMÍREZ, J.F, FLORES-MENA, J.E, Morín-Castillo, M.M. Structural characterization of CdS doped with Pb^{2+}. ECORFAN Journal-Ecuardor 2016, 3-5: 19-28

* Correspondence to Author (email: joel_diaz_reyes@hotmail.com)
† Researcher contributing first author.

Introduction

The development of third-generation solar cells overcoming the Shockley−Queisser efficiency limit for a single absorber, 31%, is one of the most fascinating challenges in the energy research field. In this aspect, semiconductor quantum dots (QDs) have shown extremely attractive properties for the development of solar cells overcoming the current limitations. The demonstration of an efficient multiple exciton generation (MEG) process in colloidal QDs, despite certain controversy, has aroused a huge interest in the use of these materials in photovoltaic devices.

This interest has been reinforced with the recent reports of absorbed photon-to-current efficiency (APCE) close to 200% and incident photon-to-current efficiency (IPCE) as high as 114%. In the former case PbS QDs have been employed in a sensitized solar cell configuration. An attempt was made to modify the band gap of CdS (~2.4 eV) by preparing a mixed lattice with a low-band-gap material, PbS (0.3 eV), giving a new set of materials, Cdl-xPbxS.

Band gaps, as low as ~1.9 eV, were achieved with increasing x. It is a semiconductor with multiple applications in the technology field for its unique properties of detection, such as infrared detectors, photoresists solar cells for their ecological aspect and the effect of multiple exciton generation was recently discovered in PbS nanostructures, which is promising for such applications, for use in electronic applications thin films transistors (TFTs). Photosensitivity of detectors can be improved by adjusting the gate voltage and in the manufacture of laser diodes by its corresponding emission spectral range 2.7-4.2 μm [1].

In this work reports the growth and characterization of CdS: Pb^{2+} nanofilms obtained by chemical bath deposition on glass substrate at low temperature. The effects of the chemical composition on structural properties of the CdS: Pb^{2+} alloy were studied by X-ray diffraction, HRTEM, EDS, Raman scattering.

Experimental details

The chemical bath is a technique to deposit and grow films on a solid substrate from a reaction that occurs in solution. It starts from an aqueous solution of salts of the elements of the compound to be obtained. It is required that the compound to deposit is relatively insoluble and chemically stable in the solution to give a simple precipitation in an ionic reaction [2].

For the synthesis of CdS: Pb^{2+}, the metal ion source is lead acetate, hydroxyl ions source is sodium hydroxide, and the sulphur source is Thiourea ions and complexing agent, ammonium nitrate. All chemical reagents were from Sigma-Aldrich unless cadmium sulphate was Merck Millipore. The feasibility of this technique for its environment is: deposit short time, it does not require high temperatures, there is no emission of toxic gases into the atmosphere and the preparation of the solutions is carried out micro scale.

For carrying out the intentional doping by lead of the deposited layers is added small lead acetate volumes to the growth solution in the range of 0 to 30 ml to obtain different lead concentrations in the nanostructures, which are presented in Table 1. The CdS:Pb^{2+} nanofilms chemical stoichiometry and surface morphology were obtained by SEM-EDS, which were carried out in a System LEO 438VP, with W.D. of 26 mm using a pressure of 20 Pa.

ISSN: 2410-4191

The crystalline phase and structure of the films were determined with a Bruker D8 Discover diffractometer using the copper Kα radiation (λ=1.5406 Å) at 40 kV and 40 mA with parallel beam geometry. HRTEM studies were carried out in a JEOL JEM200 of 80-200 KV, the obtained image is recorded with a CCD camera in real time. The Gatan Digital Micrograph software was used for the analysis of HRTEM images. Raman scattering experiments were performed at room temperature using the 6328 Å line of a He-Ne laser at normal incidence for excitation. The light was focused to a diameter of 6 μm at the sample using a 50x (numerical aperture 0.9) microscope objective. The nominal laser power used in these measurements was 20 mW.

Results and discussion

The chemical composition of the CdS: Pb^{2+} films was estimated by EDS measurements, which besides allow to know the presence of some residual impurities. The EDS results indicate that besides the samples contain a significant amount of silicon, potassium, calcium, sodium and oxygen, and other residual impurities. Thus, the most of residual impurities detected in the layers come from of the substrate, which is corning glass.

The results of such measurements are shown in Table 1, in which is included the atomic and mass percentages. From these results is observed that sample M1, CdS, is not a stoichiometric compound and that starting from it a higher thiourea concentration in the solution gives a higher presence of cadmium and lead in the material and an absence of sulphur. Continuing with the consideration that each unit cell of CdS contains two cadmium atoms and two sulphur atoms, the atomic weight of the ideal unit cell is ~288.95 corresponding to 22.19% sulphur atoms and 77.81% cadmium atoms.

Then, when a stoichiometric deviation of ideal unit cell occurs, it could establish a correspondence between vacancies or interstices of some of the compound elements (VS, VCd, Cdi, Si). In case of M1, it has excess of Cd and absence of sulphur, which is indicative that cadmium is interstitial and there are vacancies of sulphur.

The average errors with which were calculated percentage masses of different elements were for cadmium 1.25%, sulphur 0.35% and for lead 0.25%. As can see in Table 1, these errors do not significantly alter the above findings. Table 1 shows that the samples contain a lower S concentration, indicating that have a high concentration of sulphur vacancies. It can induce that there is a high concentration of cadmium and lead interstices. Therefore, the samples studied; there is excess elements II and IV and lack element VI.

Sample	$Pb(C_2H_3O_2)_2$ added volume (ml)	Cd mass weight (%)	Cd molar fraction (%)	S mass fraction (%)	S molar fraction (%)	Pb mass fraction (%)	Pb molar fraction (%)
M1	00	82.01	56.53	17.99	43.47	0.00	0.00
M2	05	74.06	52.33	18.26	44.21	7.68	3.45
M3	10	73.03	51.69	15.79	42.74	11.18	5.58
M4	15	61.19	48.29	12.71	38.10	26.10	13.61
M5	20	58.68	47.12	11.38	38.14	29.94	14.70
M6	25	56.90	45.83	11.27	38.46	31.83	18.72
M7	30	56.47	41.16	11.23	39.17	32.81	19.67

Table 1 Summary of the CdS:Pb^{2+} samples grown and studied in this work. The Pb, Cd and S concentrations in deposited samples were estimated by EDS

Figure 1a shows XRD patterns of CdS:Pb^{2+} nanofilms with different lead concentrations deposited at a temperature of 20±2°C. It is observed from XRD patterns that CdS:Pb^{2+} films deposited are in polycrystalline nature. It can be seen that each peak corresponds fairly well with data of CdS: Pb^{2+} marked in the software DICVOL04 data.

ISSN: 2410-4191

The obtained structural parameters with the software DICVOL04 data are in good agreement with the published ones. From this close agreement, it is confirmed that as deposited CdS:Pb^{2+} nanofilms for all the thiourea concentrations belong to the cubic crystal system. The X-ray patterns of deposited CdS:Pb^{2+} thin films are described in the Fm-3m(225) and whose latticeparameters were calculated using the software DICVOL04, obtaining the following lattice parameters values: a = 5.73 Å, which are in agreement with the reported values [3]. CdS exists in two crystalline modifications: the wurtzite (WZ) [4] and zinc blende (ZB) phase.

As can be seen, the obtained diffraction pattern for sample M1 shows a predominant peak at 2θ = 26.81°, which can be assigned to (111) plane of ZB CdS phase. Moreover, the intensity weak of peak at 2θ = 28.27° is due to diffraction from the (101) plane WZ phase whereas at 2θ = 26.44° position can be co-occupied by the (111) plane of ZB phase as well as the (002) plane WZ. However, the maximums peak intensity for both crystalline phases are different, ZB maximizes at 2θ = 26.81° corresponding to the (111) plane, whereas WZ phase has its maximum intensity peak at 2θ = 28.20° corresponding to (101) plane [5].

Formation of the WZ phase is likely, at least to large extent, because the characteristic diffraction peak from the (002) planes of the structure was completely absent when the CdS film was deposited. The shift in the diffraction angles are due to the incorporation of Pb^{2+} at the sub-lattices sites of Cd^{2+}. It has been reported in the literature that the probability that CdS dissolves in the PbS lattice at room temperature is very low [6]. In this case of extremely small particles, where the contribution of surface free energy is very important, some deviations cannot be excluded.

From XRD patterns can be assured that the Pb^{2+} forms PbS according to the peak observed at 2θ~30.01° in M5 and M6 samples. Besides, it is observed a widening at the peak of the preferential (111) direction, which could be caused by undergoing stress, size of small crystalline domain or fluctuations in concentration. The first case does not happen since the used substrate is amorphous and it does not produce a mismatch in the material lattice parameters. The variation in the size of the average crystalline domain is the cause of this widening that can be due to the small size of the crystals

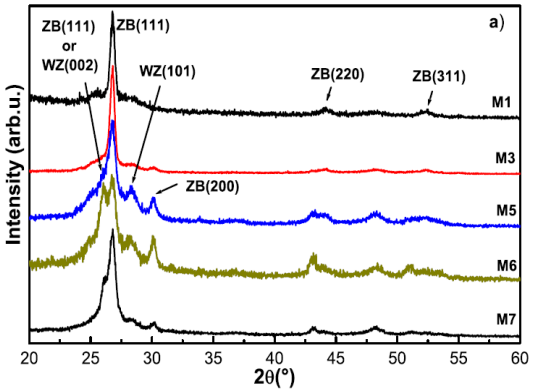

Figure 1 XRD diffraction patterns for CdS and CdS:Pb films. M1 diffractograms displays peaks at: 2θ = 26.81, 44.16 and 52.44°, which are related to the (111), (220) and (311) reflection planes for the CdS. ZB phase

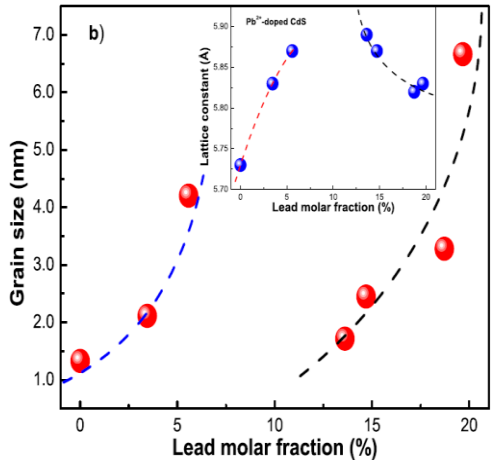

Figure 2 Dependence of the grain size of the average crystalline domain based on the increase of lead molar fraction for the CdS:Pb^{2+} system. The inset shows lattice constant as function of Pb molar fraction

And by presence of strains that possess multiple facet diffraction peaks, which is the result of multidirectional growth of the synthetized nanocrystals. In fact to apply the Debye-Scherrer equation [7], one finds that the crystalline domain increases. The mean grain size was calculated from cubic (111) reflection of CdS:Pb^{2+} for the all the studied samples. It is worth-noting the values of electronegativity for Pb (2.33) and Cd (1.69), which are favourable to form a solid solution [8].

These results show that the grain size increases as the thiourea concentration is increased in the growth solution as can be observed in Table 1 and Fig. 1a. Fig. 1b shows the variation of the size of the average crystalline domain with the lead incorporation obtained by the Debye-Scherer equation through the measurement of the width at half-maximum (FWHM) of the more intense peak that is (111) direction of deposited layers, which is sited about 26.81°. The intensity of this peak depends lightly of the lead molar fraction in the nanofilms.

The dash lines are some figures-of-merit for following the behaviour of experimental points, as is observed there are regions, the first one corresponds at low lead concentrations, M1, M2 and M3 samples, and second one to high lead concentrations, where clearly is observed the Pb^{+2} effect to replace Cd ions of the CdS:Pb^{2+} lattice. Similar behaviour is observed for the lattice constant, as shown in the inset of Fig. 1b. For the interplanar distance (ID) (111) for the ZB phase presented in Table 2, calculated from the 2θ peak position, versus lead molar fraction, increases lightly. This ID, in practice, coincides with (111) ID of the ZB phase. It can be seen that it increases as V [Pb^{+2}] increases, suggesting the formation of a solid solution and then it goes up again, having a region of discontinuity, for higher V [Pb^{2+}].

This is consistent with a single phase material at lowest V [Pb^{2+}] and a two-phase material at higher V[Pb^{2+}]. Moreover, the lattice constant increases with increasing V[Pb2+] in the film which is an effect of Pb^{2+} substituting Cd2+ in CdS. A possible explication to this experimental fact can be due to difference of the ionic radii of Cd^{2+} (0.97 Å) and Pb^{2+} (1.20 Å). The (111) ID of ZB phase in bulk are 3.367 Å.

These values are larger than the ID values found for the CdS-CdSPb films in this work. It is probable that values of ID in CdS:Pb^{2+} nanofilms are owing to the existence of Cd^{2+} vacancies.

ISSN: 2410-4191

For a relative low concentration of Pb^{2+} ion, this can be, in a large majority, be situated in: (a) Cd^{2+} vacancies sites which otherwise would be empty [9], (b) in Cd^{2+} sites provoking the appearing of Cd^{2+} interstitial, and (c) in interstitial positions. For higher V [Pb^{2+}], the material behaves like a solid solution, the generation of Cd^{2+} vacancies, whose creation is needed to charge balance, start to be important in number and given the relative ionic radius of S^{2-}.

There is a tendency of the Full Width at Half Maximum (FWHM) of (111) peak [2] of the grown films probably due to all of the possible Pb^{2+} species present in Cd^{2+} sites and interstitials positions, and also to the existence of PbS, which distort the crystalline lattice and provoke structural disorder. The distortion produces a strong strain that affects the

Sample	$a_{X\text{-}ray}$ (Å)	$d_{(111)}$ (nm)	Grain size (X-ray) (nm)	Grain size (TEM) (nm)	Bandgap I (eV)	Bandgap II (eV)	Bandgap III (eV)
M1	5.73	0.28	2.12	5.11	2.49	1.67	0.98
M2	5.83	0.29	1.33	--	2.45	1.97	2.09
M3	5.87	0.29	1.21	5.50	2.44	1.96	2.06
M4	5.89	0.31	1.72	---	2.49	1.99	2.01
M5	5.87	0.33	2.45	5.85	2.46	1.84	
M6	5.84	0.33	3.28	3.50	2.34	1.77	
M7	5.83	0.33	6.67	--	2.27	1.71	

Table 2 The mean grain sizes of the nanofilms obtained by the Debye-Scherrer equation for the direction ZB (111), which show the dependence of the grain size of the average crystalline domain based on the increase of Pb molar fraction for the CdS:Pb^{2+} system. Besides, it presents the grain sizes obtained by TEM. Additionally, it is shown the interplanar distance

Interatomic distances; this similar fact has already been reported [10]. In this work, the strain and distortion of the lattice can be smaller. The appearing of S^{2-} ions into the material favours the relaxing of the lattice. Fig. 2 illustrates images obtained by high-resolution transmission electron microscopy for some typical samples, and the insets are the result of the processing of the HRTEM image using filters in Fourier space.

As is observed in figures there is two structure types, at low V[Pb^{2+}] the crystal nanostructures are nearly spherical shape of the material with an average size of ~1.33-6.67 nm, and to the sample with higher V[Pb^{2+}] contains nanostructures boxes shape, whose dimensions are approximately (11.30-12.82) nm×(6.32-8.72) nm, see Fig. 2d. This behaviour has been observed in other materials, that by changing the concentrations of the precursors or the experimental conditions the nanoparticles shape changes.

The most direct way of controlling the reaction kinetics, and thus particle shape, in these syntheses is by changing the concentration of the lead reducing agent. Increasing the amount of lead in the growth solution increases the rate of lead ion reduction, which should create a preference for the growth of more kinetically favourable (or less thermodynamically favourable) particle morphologies [11]. In addition in the insets can see clearly the distance interplanar of material, which corresponds to the direction of the cubic phase of the CdS:Pb^{2+} (111). As can be seen, the results obtained by HRTEM are in good agreement with the results calculated from XRD using the Debye-Scherrer equation.

ISSN: 2410-4191

The structural characterization of the synthesized CdS nanostructures was therefore carried out using Raman spectroscopy. Each of the phonon wavenumbers was extracted by fitting the Raman spectrum to a Lorentz line shape, and the first longitudinal optical (1LO) and second longitudinal optical (2LO) phonons and multiphonon processes can be clearly observed in Figure 3a, which correspond a zincblende (ZB) crystalline phase. For a better analysis the Raman spectra will be divided into two frequency ranges.

The first region for frequencies below 200 cm-1 and the second one to higher frequencies as are illustrated in Figs. 3b-c, in which Raman spectra of three typical samples, M1, M2 and M7, are displayed. In Fig. 3b illustrates the CdS:Pb^{2+} Raman spectra in the range from 50 to 200 cm-1 for the three typical samples, M1, M2 and M7, showing three vibrational bands, which depend strongly on the lead molar fraction. Besides, it is observed that these bands happened a blue shift as lead concentration is increased. Similar vibration modes were obtained by Raman theories and are in agreement with the results reported by de Wijs et al. [12]. They are the typical characteristic peaks of the zincblende phase at low frequencies that were obtained by deconvolution using Lorentzian curves for finding the peaks frequency that are associated to

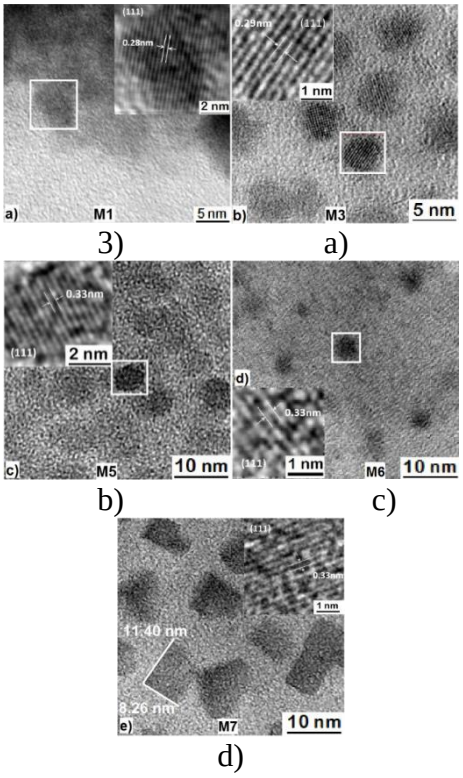

Figure 3 HRTEM micrographs of the CdS:Pb^{2+} samples: a) M3, b) M5, c) M6 and d) M7

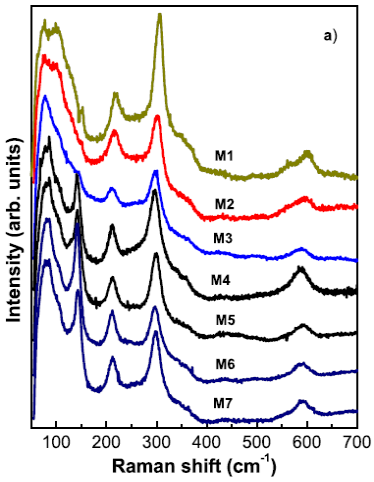

Figure 4 a) Raman spectra of the CdS:Pb^{2+} films added with different lead concentrations. Deconvolution of the spectra for two Raman shift ranges: (a) lower one and (b) higher one

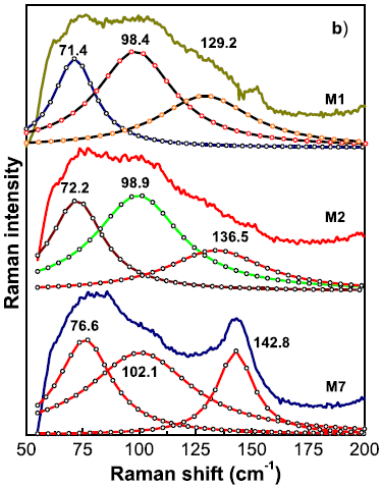

Figure a)

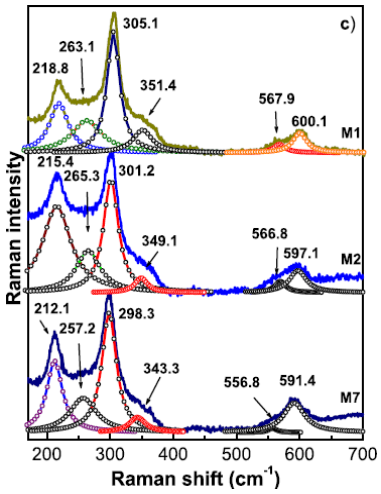

Figure b)

Lattice modes [13]. As is observed in Figs. 3, from M4-M7 Raman spectra the peak about 143 cm-1 is well-resolved and can be associated to the combination of longitudinal and transverse acoustic phonon modes in PbS nanocrystals [14]. Then, the second frequency region will be discussed. The Raman peaks of M1 (nanoparticles) appear at 305.1 cm-1, attributed to the A1(LO) mode with a full width at half maximum (FWHM) of ca. 24.3 cm-1 and its overtone at 600.2 cm-1. The Raman peaks of M2 (nanoparticles) appear at 301.2 cm-1 with a FWHM of ca. 28.3 cm-1 and its overtone at 597.1 cm-1.

The Raman peaks of M7 (nanoparticles) appear at 298.3 cm-1 with a FWHM of ca. 28.1 cm-1 and its overtone at 591.4 cm-1 [15]. As is observed of these results Raman peaks are redshifted as lead concentration is increased in the nanofilms and the Raman spectra exhibit relatively sharp crystal-like peaks. The light increase of the FWHM from M1 to M2 and M7 can be attributed to a slight deterioration of the crystallinity of the CdS nanocrystals due to the incorporation of lead to Cd sub-lattice. It has been reported that defect-free crystalline CdS films have a FWHM of 8 cm-1 [16].

Therefore, grown samples have a high density of structural defects, as had been deduced from the results of the chemical composition. We all know that in a crystalline semiconductor or insulator the observed Raman shifts usually correspond to the LOs, whereas other modes such as the transverse optical and surface phonon modes are not observable because of symmetry restrictions and their low intensities [17]. Another observation is that the peak profile of the nanoparticles is almost symmetric for the three samples.

It is also observed that the intensity of the Raman line LO of sample M2 is lower than that of M1, which is attributed to the quantity of the sample detected by Raman, see Fig. 4a. It is known that the intensity of a Raman line is proportional to the number of scattering centres because of the fact that Raman scattering is an incoherent process [18], in this case, as can be seen in Fig. 4b, the lattice vibrational frequencies are dominant and shielding to the longitudinal optical vibrations, as the V[Pb^{2+}] increases.

In addition to the LO phonon and its replicas, and lattice vibrations, for sample M1, several peaks are resolved as 263.1, 351.4, and 567.9 cm−1 suggesting that the samples have better crystalline quality [19].

ISSN: 2410-4191

The peaks at approximately, 263.1, 351.4 and 567.9 cm−1 can be assigned to multiphonon scattering, which is consistent with other reports [20]. The feature at the high-energy shoulder, sited at 351.4 cm-1, is the subject of a recent study by Dzhagan et al. [21], who suggest that it results from the participation of acoustic phonons to the scattering process and the mode corresponding to the low-energy shoulder originates from surface optical phonon modes (SO) at 263.1 cm-1 [22]. As is observed in Figs. 4b-c, the frequencies of the vibrational bands decrease as the lead molar fraction increases, this is consistent because of the ionic radius of lead is higher than cadmium.

Conclusions

In this work presented the growth and characterization of CdS:Pb^{2+} nanofilms obtained by CBD technique by under our proposed reactant species and at 20 ±2°C as deposited temperature. The results of the studies of X-ray diffraction and Raman spectroscopy showed that grown CdS:Pb^{2+} nanofilms belong to the zincblende crystalline systems. The mean grain sizes of the nanocrystals are in the range of 1.21-6.67 nm, which were determined using the Debye-Scherrer equation for the ZB(111) direction and that were confirmed by HRTEM, although with this technique were obtained larger sizes.

This mean grain size indicates a high quantum confinement. Raman scattering showed that the lattice dynamics is characteristic of bimodal behaviour and the multipeaks adjust of the first optical longitudinal mode for the CdS:Pb denotes in all cases the Raman frequency of the characteristic peak is in the range of 305-298 cm-1 of the CdS nanocrystals associated with the lead.

References

[1]Jeff Hecht, Understanding Lasers, 2nd ed., IEEE Press, New York NY(USA), 1994.

[2]J.I. Contreras-Rascón, J. Díaz-Reyes, J. E. Flores-Mena, M. Galván-Arellano, L. A. Juárez-Morán, R. S. Castillo-Ojeda. Curr. Appl. Phys. 15 (2015) 1568

[3]J. Singh. Physics of Semiconductors and their heterostructures. Ed. McGraw-Hill, 1993.

[4]A. Abdolahzadeh Ziabari, F. E. Ghodsi. J. Lumin. 141 (2013) 121.

[5]G. Murugadoss. Superlattice Microst. 52 (2012) 1026.

[6]M. Guglielmi, A. Martucci, J. Fick, G. Vitrant. J. Sol-Gel Sci. Technol. 11 (1998) 229.

[7]J. A. Dean, Lange's. Handbook of Chemistry, 13th ed. (New York: McGraw-Hill. 1987).

[8]R. Ortega-Borges, D. Lincot. J. Electrochem. Soc. 140 (1993) 3464.

[9]M. Grus, A. Sikorska. Physica B: Condensed Matter 266 (1999) 139.

[10]M. Esmaili, A. Habibi-Yangjeh. Chin. J. Catal. 32 (2011) 933.

[11]M. R. Langille, M. L. Personick, J. Zhang, Ch. A. Mirkin. J. Am. Chem. Soc. 134 (2012) 14542.

[12]G. A. de Wijs, R. A. de Groot. Electrochim. Acta 46 (2001) 1989.

[13]A. Rougier, F. Portemer, A. Quédé, M. El Marssi. Appl. Surf. Sci. 153 (1999) 1.

[14]G. D. Smith, S. Firth, R. J. H. Clark, M. Cardona. J. Appl. Phys. 92 (2002) 4375.

ISSN: 2410-4191

[15]E. J. Donahue, A. Roxburgh, M. Yurchenko. Mater. Res. Bull. 33 (1998) 323.

[16]M. Froment, M. Claude-Bernard, R. Cortes, B. Mokili, D. Lincot. J. Electrochem. Soc. 142 (1995) 2642.

[17]K. K. Nanda, S.N. Sarangi, S.N. Sahu, S.K. Deb, S.N. Behera. Physica B: Condensed Matter 262 (1999) 31.

[18]H. Brunner, H. Sussner. Biochim. Biophys. Acta 271 (1972) 16.

[19]V. Sivasubramanian, A.K. Arora, M. Premila, C.S. Sundar, V.S. Sastry. Physica E: Low-dimensional Systems and Nanostructures 31 (2006) 93.

[20]S. Kar, B. Satpati , P. V. Satyam, S. Chaudhuri. J. Phys. Chem. B 109 (2005) 19134.

[21]V. M. Dzhagan, I. Lokteva, M. Ya. Valakh, O. E. Raevska, J. Kolny-Olesiak, D. R. T. Zahn. J. Appl. Phys. 106 (2009) 084318.

[22]F. Comas, Nelson Studart, G.E. Marques. Solid State Commun. 130 (2004) 477.

ISSN: 2410-4191